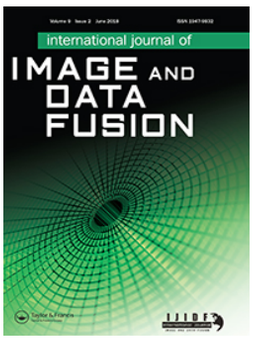

International Journal of Image and Data Fusion

ISSN: 1947-9832 (Print) 1947-9824 (Online) Journal homepage: https://www.tandfonline.com/loi/tidf20

# Performance measurement without ground truth to achieve optimal edge

Cahyo Crysdian

**To cite this article:** Cahyo Crysdian (2018) Performance measurement without ground truth to achieve optimal edge, International Journal of Image and Data Fusion, 9:2, 170-193, DOI: 10.1080/19479832.2017.1384764

**To link to this article:** https://doi.org/10.1080/19479832.2017.1384764

Published online: 06 Oct 2017.

INTERNATIONAL JOURNAL OF IMAGE AND DATA FUSION, 2018
VOL. 9, NO. 2, 170–193
https://doi.org/10.1080/19479832.2017.1384764

Taylor & Francis
Taylor & Francis Group

RESEARCH ARTICLE



# Performance measurement without ground truth to achieve optimal edge

Cahyo Crysdian

Department of Computer Science, Universitas Islam Negeri Maulana Malik Ibrahim Malang, Malang, Indonesia

**ABSTRACT**

This paper presents an effort to develop performance measurement of edge detector without ground truth. The motivation is to drive edge detector to catch up with human vision that is capable of always generating closed-loop edge. Two axioms of edge are presented, i.e. the presentation of edge as a closed-loop line and its characteristic as being thin. A set of features and approaches are generated in this research in order to enable the measurement of edge map. Experiment shows that current edge detector is still difficult to catch up with human vision for recognising edge. Experiment also proves that statistical approach based on object size delivers the best performance measurement among other approaches. And, the use of region of interest is proved useful to optimise edge measurement.

**ARTICLE HISTORY**
Received 5 June 2017
Accepted 13 September 2017

**KEYWORDS**
Performance measurement; edge detector; edge map; human vision; statistical approach; multi-criteria decision-making

## 1. Introduction

Performance measurement of edge map has always been a hot topic to research due to vital role of edge detector to simplify image data. Indeed, edge detection has widely been recognised having similar role with edge perception in human vision. It has been known that the way human recognises object from visual data is started by extracting the edge of object (Papari and Petkov 2011). Unlike human visual system which has capability to extract high accurate edges of even complicated objects in only milliseconds (Oliva and Torralba 2006), currently it is still difficult for machine to obtain optimal edge from natural objects in digital image. The term 'optimal edge' here refers to a complete closed-loop edge surrounding the shape of object. This statement is consistent with the definition of edge obtained from some well-known English dictionaries such as Longman, MacMillan and Collins COBUILD. In these dictionaries, edge is defined as a set of furthest points of an object from its centre. It means projecting edge point to all directions would create a closed-loop line that represents object boundary. It is worth to note that achieving closed-loop edge would greatly facilitate any further image analysis processes.

The definition above is consistent with Koren and Yitzhaky (2006) that defines edge as boundary between object and its background. This definition is also

**CONTACT** Cahyo Crysdian cahyo@ti.uin-malang.ac.id Department of Computer Science, Universitas Islam Negeri Maulana Malik Ibrahim Malang, Malang, Indonesia

consistent with Verma *et al*. (2011) that states the existence of edge is marked with discontinuities or significant variation in intensity or grey levels of image. Based on the last two definitions, we argue that the definition of edge by Abdou and Pratt (1979) stating that edge is a local change or discontinuity in image attributes, such as luminance, intensity or texture, is not necessarily an edge. In this case, any local change in intensity or other local attributes in an image is only the indication of the presence of edge. There is a room of possibility that they do not represent the edge of an object. Perhaps, there are other parts of image which are more closely related to them such as noise or any inside content of the object. Therefore in this research, the definition of edge by Koren and Yitzhaky is expanded to become 'edge is the boundary between adjacent objects or between an object and its background'.

Beside tremendous development of edge detection that has been achieved up to now (Oskoei and Hu 2010, Papari and Petkov 2011), currently people and their machine involve in tedious works to extract optimal edges for even simple natural object. The works usually include enhancing the input image, selecting and employing edge detection methods from dozens that have been proposed in this field, up to generating ground truth for comparison in order to select the most optimal edge from hundreds of possible results. The last task, i.e. ground truth generation, undoubtedly requires prior knowledge to recognise the objects composing digital image. It is worth to note that ground truth usually is supplied through user intervention. Hence, obtaining automatic process in order to deliver optimal edge becomes a challenging task to achieve. Automation shall be capable of employing various methods which include their combination and derivatives. We argue that it would not be possible for a single method of edge detection to derive optimal edge of varied objects from natural image scene. It is due to varied sensitivities of edge detector algorithms to recognise object boundaries. Hence, intervention should be given without disturbing automatic process of edge detection. It means no prior knowledge or manual action such as comparison with ground truth is allowed to interrupt the operation of edge detector.

Researchers have indeed been working to achieve optimal edge by employing performance measurement as depicted in Figure 1. Some methods have been proposed and few have still been used even today despite the raising question of their performance (Abdou and Pratt 1979, Besuijen and Heyden 1989, Baddeley 1992, Hidalgo and Massanet 2011). It is worth to note that current performance measurement still put respect on the existence of open-loop edge (Gimenez *et al*. 2014). This practice certainly violates the definition of optimal edge above. Therefore, this paper aims to extend performance measurement in order to achieve the delivery of optimal edge as a closed-loop boundary.

The rest of the paper is organised as follows. Section 2 delivers related works in the field of performance evaluation of edge detector. Section 3 presents our approach to reshape edge as a closed-loop line in order to represent the boundary of object. This section is to facilitate the development of performance measurements without ground truth that are presented in Section 4. Experiment, discussion and enhancement of the presented method are given in Section 5. The works of this research are concluded in Section 6.

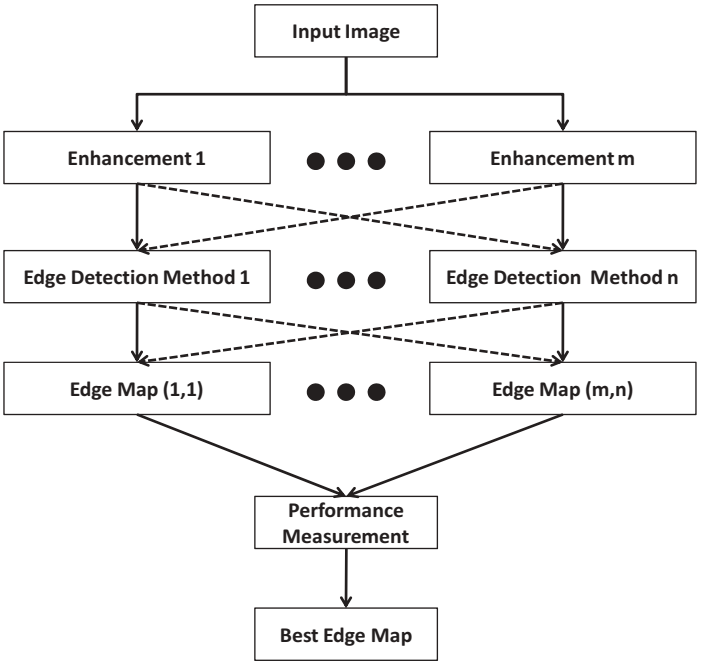


**Figure 1.** Performance measurement to deliver optimal edge.

## 2. Related works

The introduction of Figure of Merit (FoM) by Abdou and Pratt (1979) became the milestone of performance measurement for edge detection. The mechanism of FoM is held by comparing an edge map derived from a detection process against a prior defined ground truth in pixel basis given as follows:

$$\text{FoM} = \frac{1}{\max\{\mathbf{EM}, \mathbf{GT}\}} \sum_{x \in \mathbf{EM}} \frac{1}{1 + \alpha d^2(x, \mathbf{GT})} \tag{1}$$

where **EM** is an edge map, **GT** is a ground truth, $d$ is Euclidean distance, $x$ is a set of pixel value and $\alpha$ is predefined value that usually is set to 1/9. Usually, the ground truth is developed by manual interpretation of object contour based on human perception, and in some cases, it involves even human experts such as medical doctor for interpreting medical images. Despite its dependency on ground truth, FoM has still been used even today due to its simplicity. However, it is difficult to always generate ground truth for random natural images. It is even impossible to incorporate this method to find the best optimum edge maps from multiple random images in automatic manner since human intervention is always required to generate ground truth. For comparison, human visual system is capable for developing edges from different visual scene without ground truth. Thus, the dependency on ground truth becomes the main drawback of this method.

Moreover, researchers disclosed other flaws of FoM such as its possibility to produce the same measurement results from different edge conditions (Besuijen and Heyden 1989, Baddeley 1992). An approach to overcome this problem was developed by

Besuijen and Heyden (1989) by proposing a mechanism to recognise a set of possible errors such as displaced pixels, superfluous edge and clustering error. Other approach to improve FoM was proposed by Baddeley (1992) that employed modified Hausdorff metric in order to introduce Δ to measure distinct quality of two binary images given by

$$\Delta_{\omega}^{p}(\mathbf{EM},\mathbf{GT}) = \left[\frac{1}{N}\sum_{x\in\mathbf{X}} |\omega(d(x,\mathbf{EM})) - \omega(d(x,\mathbf{GT}))|^{p}\right]^{1/p} \tag{2}$$

where $N = n(X)$ as a total number of pixels in the raster $\mathbf{X}$ in which $\mathbf{EM}, \mathbf{GT} \subseteq \mathbf{X}$, $\omega$ is a concave continuous function and $p$ is the order of mean difference. Later, Hidalgo and Massanet (2011), however, empirically proved that FoM still outperformed Baddeley's Δ metric.

Ji and Haralick (1999) developed different approach to employ indirect performance measurement by calculating the variance of convolution kernel rather than directly evaluating the edge map. Although the performance of different convolution kernels could be recognised by this approach, it did not represent real performance of edge detector to extract edges particularly for random images. It would be difficult to employ this metric to disclose the quality of edge map, i.e. whether the edge map contained edges which appropriately represented or inappropriately violated image content.

Later, Yitzhaky and Peli (2003) utilised a statistical approach to build correspondence between different edge maps that were produced by different treatments to input image. The correspondence was employed to build estimated ground truth based on dominant selection of edge pixels. This effort was noted as the first method to directly evaluate the performance of edge map without ground truth. However, this method was prone to error since different algorithm of edge detector has been known having different sensitivity to recognise edge. If somehow there was condition where more edge detectors missed edge pixels due to blurry intensities or noisy image, while in fact the pixel actually represented the boundary of object, this pixel would not be considered as significant edge even though they represented the actual object. Moreover, evaluation of edge map was established at pixel level. Thus, it was not possible to recognise the structure of the edges, i.e. whether they really represented the object shapes or just noise. The work was then continued by Koren and Yitzhaky (2006) to improve the performance of Yitzhaky and Peli by introducing saliency map based on spatial approach in order to develop estimated ground truth. However, the result was indifferent to Yitzhaky and Peli since the probability that edge pixel represented noise was actually very high. Moreover, the results also showed the existence of many uncompleted edges that did not completely surrounding the objects of image. It was due to the missing of edge structure analysis.

Recently, Gimenez *et al*. (2014) proposed a statistical complexity measure to evaluate the quality of edge map in which complexity $C$ is defined as a combination of equilibrium index $\varepsilon$ and entropy index $\mathcal{H}$. For edge map **EM**, complexity is given by

$$C = \varepsilon(\mathbf{EM})\mathcal{H}(\mathbf{EM}) \tag{3}$$

where equilibrium is obtained by $\varepsilon(\mathbf{EM}) = (1/|\mathbf{EM}|)\sum_{k=1}^{|\mathbf{EM}|}\mathcal{Q}_{\mathfrak{B}}(\mathbf{EM}_k)$ with $|\mathbf{EM}|$ which is the cardinal number of the set of all pixels in **EM**, and $\mathcal{Q}_{\mathfrak{B}}(\mathbf{EM}_k) = \max_{1 \le j \le n}\left(\mathbf{b}_j^T\mathbf{EM}_k/\mathbf{b}_j\mathbf{EM}_k\right)$ for a collection of $N \times N$ edge patterns obtained from Bresenhaum data set represented by $\mathfrak{B} = \{\mathbf{b}_1, \mathbf{b}_2, \ldots, \mathbf{b}_n\}$ that are being slid over the edge map **EM** centred in each edge pixel at position $k$, thus it operates on edge sub-maps $\mathbf{EM}_k$. The use of edge patterns here is to replace ground truth in order to conduct comparison with known edge structures. Meanwhile, entropy index is computed as $\mathcal{H}(\mathbf{EM}) = 1 - \mathcal{D}(\mathbf{EM})$ with $\mathcal{D}(\mathbf{EM}) = \max_{(x,y)\in\mathbf{R}^2}|F_{\mathbf{EM}}(x,y) - F(x,y)|$ and $F_{\mathbf{EM}}(x,y) = (|\{(i,j) \in \mathbf{EM}|\phi_1(i) \le x.\phi_2(j) \le y\}|/|\mathbf{EM}|)$ in which $(i,j) \in \mathbf{EM}$ for $N \times M$ image size and $\phi(i,j) = (\phi_1, \phi_2) = ((2i - 1/2N), (2j - 1/2M))$. $F(x,y)$ is the cumulative distribution function of a uniform distributed bidimensional vector. Although it is independent from ground truth, this method is prone to the missing of edge patterns. Moreover, experiment shows the delivery of many insignificant edges in term of short and open-loop edges due to entropy index. This method however is noted as the first performance evaluation without ground truth that analyses the structure of edges.

Ornelas *et al*. (2015) proposed fuzzy index for performance evaluation. They argued that current methods of edge performance evaluation discard critical information contained in pixel level since they normally operate in edge map which is known as a binary image. The applicability of this method however is still questionable since it was tested only on synthetic images. Moreover, this method still depends on ground truth just like its predecessor.

## 3. Edge presentation

The goal of this section is to develop edge presentation as defined by Section 1. The work consists of three stages, namely edge and non-edge indexing, open-loop edge removal and edge thinning elaborated as follows.

### 3.1. *Edge and non-edge indexing*

Indexing edge and non-edge as two distinct components composing edge map is an initial step towards edge map measurement. Here, edge refers to all pixels composing edge map that are identified by edge detector as edge, while non-edge refers to all other pixels that are not identified as edge. Let $\mathbf{e}_1, \ldots, \mathbf{e}_n$ become a set of edges **PE** existed in an edge map **EM**, and let $\mathbf{o}_1, \ldots, \mathbf{o}_m$ become a set of non-edge that represents a set of objects **PNE** existed in the same edge map; hence, $\mathbf{PE} = \{\mathbf{e}_1, \ldots, \mathbf{e}_n\}$, $\mathbf{PNE} = \{\mathbf{o}_1, \ldots, \mathbf{o}_m\}$, **PE**, **PNE** $\subseteq$ **EM**, **PE** $\cup$ **PNE** = **EM** and **PE** $\cap$ **PNE** $= \emptyset$. An edge $\mathbf{e}_a \subseteq$ **PE** is defined as a set of adjacent pixels in the domain of **PE** that contain index $a$ with $1 \le a \le n$. Similarly, a non-edge $\mathbf{o}_b \subseteq$ **PNE** is defined as a set of adjacent pixels in the domain of **PNE** that contain index $b$ with $1 \le b \le m$.

### 3.2. *Open-loop edge removal*

Gestalt principle on closure (Desolneux *et al*. 2008) states that human tends to perceive the edge of every object as a closed boundary. This statement is consistent with the definition of edge given in Section 1 and become the motivation to treat edge as a closed-loop boundary of object. Therefore, the presentation of edge must always be in the form of a closed-loop line (Axiom 1). Based on this axiom, any open-loop line could not be considered as edge since they violate the basic principle of edge as closed boundary of object. Removing any open-loop edge contained in an edge map is required to fulfil the definition of edge as stated in Section 1. Thus, any pixels composing open-loop line is converted to become object or non-edge component. Meanwhile, the closed-loop line would be preserved as edge component as follows. Let **CE** and **CNE** denote a set of closed-loop edge and a set of expanded non-edge components, respectively, contained in an edge-map **EM**. Hence, **CE**, **CNE** $\subseteq$ **EM**, **CE** $\cup$ **CNE** = **EM** and **CE** $\cap$ **CNE** = $\emptyset$. Any pixel $p_i \in$ **EM** will be preserved as **CE** if it fulfils the equation given by

$$\mathbf{CE} = \{p_i | p_i \in \mathbf{PE}, |\mathbf{Ne}_i| > 1, \mathbf{Ne}_i \subset \mathbf{PNE}\} \tag{4}$$

where $\mathbf{Ne}_i$ denote a set of adjacent objects or non-edge components surrounding $p_i$. Therefore, $|\mathbf{Ne}_i|$ is the magnitude of $\mathbf{Ne}_i$ or the number of objects composing the neighbour of $p_i$. Conversely, **CNE** is given by

$$\mathbf{CNE} = \mathbf{PNE} + \{p_i | p_i \in \mathbf{PE}, |\mathbf{Ne}_i| \leq 1, \mathbf{Ne}_i \subset \mathbf{PNE}\} \tag{5}$$

Equations 4 and 5 state that every edge pixel is preserved as edge if it is located next to at least two neighbouring objects; otherwise, it is converted as a part of an object. Running Equations 4 and 5 to an open-loop line that contains closed-loop edge such as presented in Figure 2(a) produces a closed-loop edge that still carries some open-loop lines such as presented in Figure 2(b). In this case, the algorithm of open-loop edge removal considers the open-loop line as a closed-loop edge that has more than a pixel width. Therefore, thinning algorithm is required to clean up the

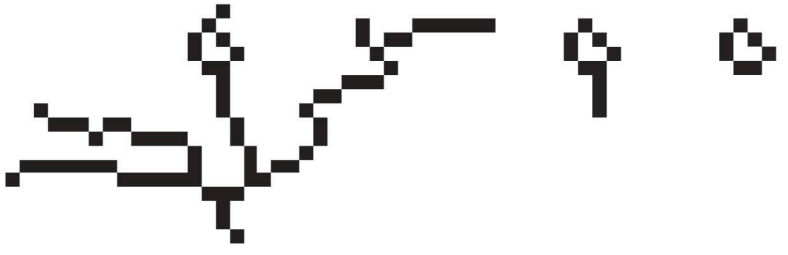


**Figure 2.** Closed-loop edge contained in an open-loop line. (a) Presentation of edge before running open-loop edge removal, (b) open-loop line presented from the result of open-loop edge removal is considered as closed-loop edge having more than a pixel width and (c) desired presentation of closed-loop edge from (a).

edge in order to get a clean presentation of closed-loop line as presented in Figure 2(c).

### 3.3. *Edge thinning*

Since edge always creates the boundary of object (referring to Axiom 1), thus in reality, it becomes an imagery line separating an object to other object or to its background. Therefore, the appearance of edge is always presented by a line that has minimum width in which edge should have not more than a pixel wide (Axiom 2). This axiom enables optimum localisation of object shape. Based on this axiom, any edge that has more than a pixel wide must undergo shrinking mechanism to reduce its width but still keeping its length. This way, any algorithm for thinning digital pattern such as Zhang and Suen (1984) could not be employed since there are possibilities that the length of edge would be reduced to a certain extent. Therefore, this axiom is achieved through the computation given by

$$\mathbf{E} = \{p_i | p_i \in \mathbf{CE}, |\mathbf{Ne}_i| > 1, \mathbf{Ne}_i \subset \mathbf{CNE}\} \tag{6}$$

$$\mathbf{NE} = \mathbf{CNE} + \{p_i | p_i \in \mathbf{CE}, |\mathbf{Ne}_i| \leq 1, \mathbf{Ne}_i \subset \mathbf{CNE}\} \tag{7}$$

where **E** and **NE** become a set of edge and a set of non-edge components, respectively, contained in edge map **EM**, in which $\mathbf{E}, \mathbf{NE} \subseteq \mathbf{EM}$, $\mathbf{E} \cup \mathbf{NE} = \mathbf{EM}$ and $\mathbf{E} \cap \mathbf{NE} = \emptyset$.

## 4. Performance measurement

Mechanism to evaluate the performance of edge detector is conducted on edge map **EM** that has undergone open-loop edge removal and thinning process as given by Equations 4–7. The strategy is to compute the performance index based on the presentation of edges $\mathbf{E} \subseteq \mathbf{EM}$ and the presentation of objects $\mathbf{NE} \subseteq \mathbf{EM}$ by computing a set of features as follows.

The first feature to compute is the length of edge that has previously been noticed by some researchers as an important parameter to justify good edge quality (Koren and Yitzhaky 2006, Gimenez *et al*. 2014). Computation to measure the length of an edge $e_a$ is given by

$$el_a = \sum_{p_i \in e_a} 1 \tag{8}$$

for $i = 1, \ldots, n$ and $e_a \subset \mathbf{E}$.

Second feature to compute is the coverage of edge that is measured as follows. Let $c_a$ become the centroid of edge $\mathbf{e}_a$ as shown in Figure 3. For every pixel $p_i \in \mathbf{e}_a$, the coverage of edge $ec_a$is computed by using Euclidean distance given by

$$ec_a = \sqrt{\sum_{i=1,\ldots,m} (c_a - p_i)^2} \tag{9}$$

Since it is desired to compute only the coverage of edge but not its length, it is necessary to eliminate the effect of the number of pixels composing each edge. It is

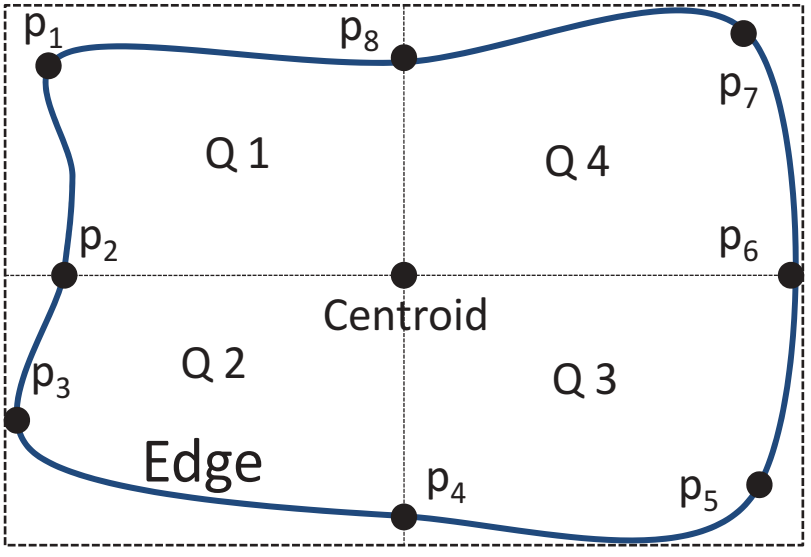


**Figure 3.** Eight pixel positions for edge coverage measurement $p_1, \ldots, p_8$.

settled by picking only eight positions of pixel from each edge to be included in Equation 9 such as depicted in Figure 3. The first four positions are defined as the far left, bottom, far right and top direction relative to its centroid which are represented by $p_2, p_4, p_6$ and $p_8$, respectively. Meanwhile, the last four positions are computed by dividing edge into four quadrants based on the position of its centroid such as illustrated in Figure 3. The next step is to determine the positions of the pixel to represent each quadrant by computing longest Euclidean distance with reference to its centroid. In this case, they are represented by $p_1, p_3, p_5$ and $p_7$ for quadrant Q1, Q2, Q3 and Q4, respectively. This strategy becomes a fair measurement for each edge being evaluated.

It is worth to note that computing the coverage of edge is important due to the condition where any pixels composing image could become a part of edge that potentially increase the length of edge; however, longer edge does not guarantee that the edge has larger coverage such as shown in Figure 4. This phenomenon reveals

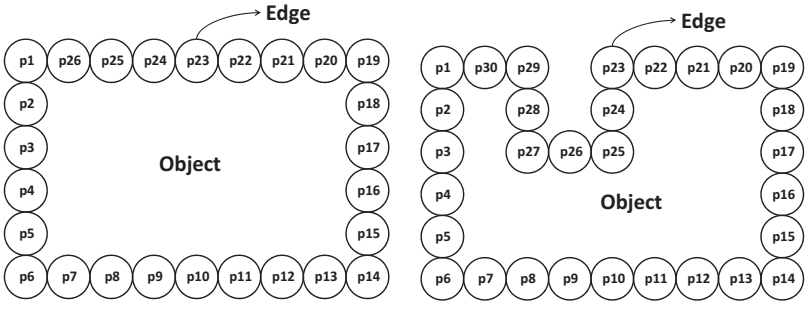


**Figure 4.** Longer edge does not always contribute to larger coverage.

the fact that the coverage of edge to some extent is independent to the length of edge. Since no open-loop edge has been left remained due to Axioms 1 and 2 as described in the previous section, any existence of edge indicates the existence of object because the edge always become the boundaries of object. Hence, the coverage of edge contributes to either the size or the number of objects existed in the image.

The third feature to compute is the size of object. Although it does not necessarily correlate to the quality of edge detection, larger size of object tends to deliver more meaningful content while small size of object mostly is produced from noise or meaningless content. Computation to measure the size of an object $os_a$ is given by

$$os_a = \sum_{p_i \in o_a} 1 \tag{10}$$

for $i = 1, \ldots, n$ and $o_a \subset \mathbf{NE}$.

The last feature to compute is the coverage of object *oc*. Computation to derive this parameter follows the mechanism to derive the coverage of edge as explained above. After deriving a set of features from edge map, two different approaches are employed for performance evaluation, i.e. statistical based and multi-criteria decision-making (MCDM) as discussed in the following section.

### 4.1. *Statistical-based evaluation*

This approach assumes that every natural image contain varied objects in different sizes. Therefore when the edges of those objects are optimally detected, the edge map most probably carries varied edges and non-edge components. If this condition is statistically measured based on the extracted feature described above, it would generate either high or low deviation value. Here, the deviation of an edge map is computed by $\sigma = (1/n)\sqrt{\sum_{i=1,\ldots,n}(f_i - \mu)^2}$ where $f$ become an extracted feature obtained from the edge map and $\mu$ is the mean of this feature. We argue that the sorted deviation value either in ascending or descending reveals the best edge map from a set of edge maps that are obtained by employing different combinations of edge detectors to an input image. This approach compares the number of feature from the top edge map obtained by ascending against the top edge map of descending in order to determine which sorting mechanism is suitable to identify the best edge map. Here, edge map with larger number of feature determines the sorting mechanism to be employed and thus the top edge map of this sorting approach become the best edge map. Hence for a set of edge map $\mathbf{EM}_1, \ldots, \mathbf{EM}_m$ having deviation $\sigma_1, \ldots, \sigma_m$, respectively, the best edge map is given by $\mathbf{max}/\mathbf{min}(\sigma_1, \ldots, \sigma_m)$.

### 4.2. *Multi-criteria decision-making (MCDM)*

This approach employs a weighted sum model to compute the performance index $\mathrm{PI} = \sum_{i=1}^{n} w_i f_i$ where $w_i$ become the weight for $i$th-feature $f$. The definition of weight is to recognise varied size of feature $f$ extracted from an edge map, in which its variation

could reach hundreds different sizes from each feature. Here, the weight assigned to each size of feature $f$ follows the famous series of Zeno dichotomy paradox as given by

$$\sum_{i=1}^{\sim} \frac{1}{2^i} = \frac{1}{2} + \frac{1}{4} + \frac{1}{8} + \cdots = \frac{1}{w_1} + \frac{1}{w_2} + \frac{1}{w_3} + \cdots = 1 \tag{11}$$

where $i$ becomes the index of feature size in descending order. The use of this series is due to the assumption that edge detector algorithm could generate infinite number of edges and objects, in which bigger size of edges and objects is worth more than the smaller one.

Meanwhile, the presentation of objects in a set of non-edge components **NE** consists of foreground and the background, where foreground represents the existence of the objects. Since the performance index aims to measure only the existence of object, it is important to exclude background from **NE**. To enable the identification of background among the existing objects $\mathbf{o}_1, \ldots, \mathbf{o}_m \subseteq \mathbf{NE}$, the computation is given as follow. Let **I** become a digital image that is composed by $x \times y$ pixels, and let **F** become a set of constants representing the minimum and maximum coordinate of **I**, thus $\mathbf{F} = \{1, x, y\}$. Let **G** become a set of $p_i \in \mathbf{o}_b$ that constructs the outside border of object $\mathbf{o}_b$ for $1 \leq b \leq m$, thus $\mathbf{G} \subseteq \mathbf{o}_b$. A classification process is applied to $\forall p_i \in \mathbf{o}_b$ as given in Equation 12 that categorises every pixels composing object $\mathbf{o}_b$ into three classes, i.e. $\alpha$ for every pixel of $\mathbf{o}_b$ that reside in the minimum or maximum coordinate of **I**, $\beta$ for every pixel constructing the outside border of object $\mathbf{o}_b$ that do not belong to $\alpha$ and void for every pixels located elsewhere.

$$p_i = \begin{cases} \alpha & \text{if } p_i \in \mathbf{F} \\ \beta & \text{if } p_i \notin \mathbf{F}, p_i \in \mathbf{G}, \exists \mathbf{Ne}_{p_i} \in \mathbf{E} \\ \text{void} & \text{if none above} \end{cases} \tag{12}$$

Based on the result of Equation 12, background identification is given by

$$\mathbf{o}_b = \begin{cases} \text{background} & \text{if}(\gamma \log \alpha \geq \log \beta) \text{ or } (|\log \beta - \gamma \log \alpha| \leq \zeta) \\ \text{object} & \text{if}(\gamma \log \alpha < \log \beta) \text{ and } (|\log \beta - \gamma \log \alpha| \leq \zeta) \end{cases} \tag{13}$$

where $\gamma$ and $\zeta$ are prior defined constants. Results for identifying background to some of USC standard image using Equations 12 and 13 with $\gamma = 4$ and $\zeta = 0.2$ are shown in Figure 5.

## 5. Experiment and discussion

Experiment to test the performance of the proposed method has been conducted to some USC standard images. It is important to note that not all images from this dataset are employed. Only images with dominant object are used for the experiment. The experiment aims to prove that the proposed method is capable of sorting the edge maps from one with the richest edges to the poorest. Achieving successful sorting is vital in this experiment since the decision for selecting the best edge map from dozen alternatives is always within the scope of rich edges. Before conducting the experiment, it is necessary to generate a set of edge maps as the input for performance evaluation. Normally, it is settled by performing the combination of a

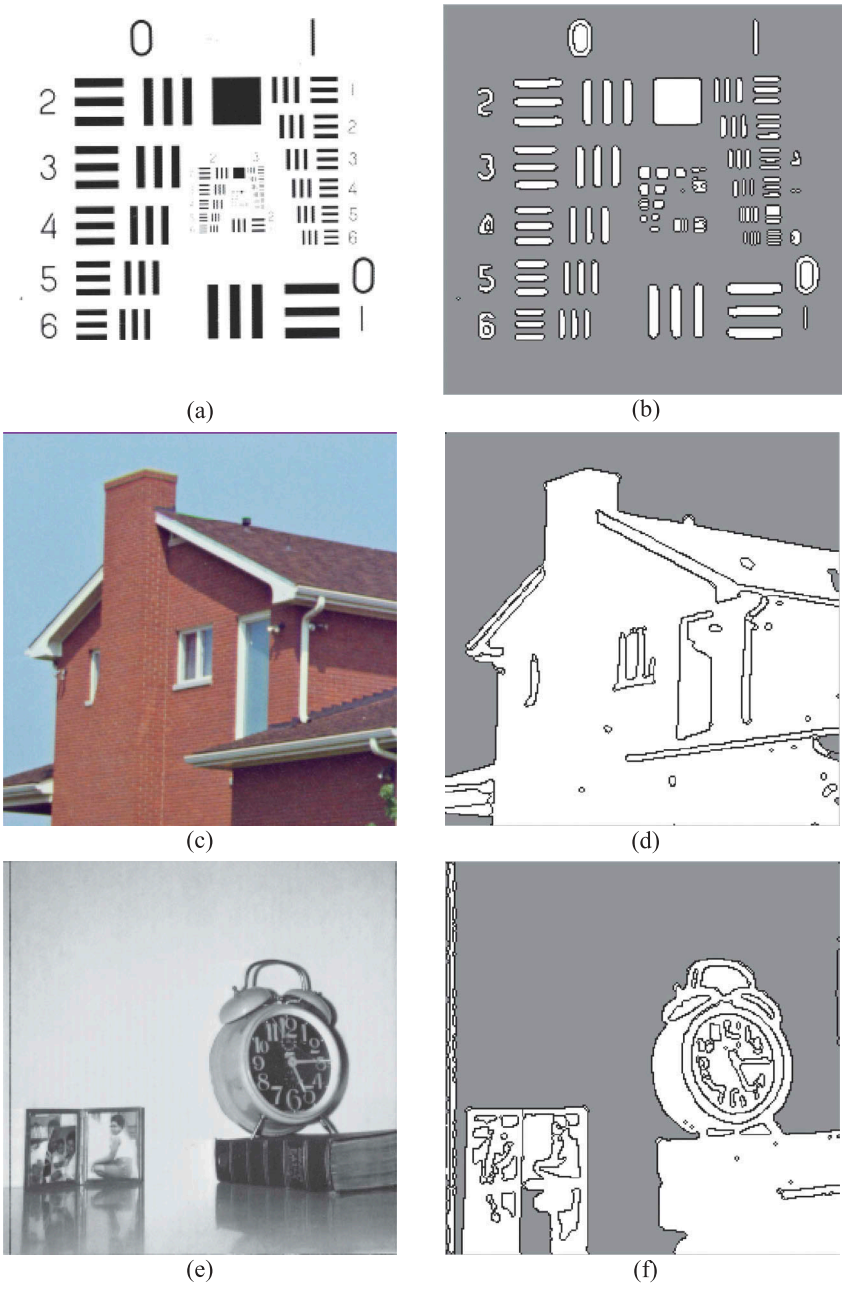

**Figure 5.** Results for background identification to some USC standard images regardless of edge detectors being employed. Figure parts (a,c,e) are input images. Figure parts (b,d,f) are the result of background identification obtained from (a,c,e), respectively. Background is presented as grey region.

set of preprocessing to a set of edge detector algorithm. Let $pr_i$ become a function of preprocessing for $i = 1, \ldots, m$, and let $ed_j$ become a function of edge detector for $j = 1, \ldots, n$, a set of edge map **EM** is produced by performing computation given by

$$\mathbf{EM}_{i\times j} = ed_j(pr_i(I)) \tag{14}$$

Thus if there exist $m$ number of preprocessing algorithm and $n$ number of edge detector, the combination would produce $m \times n$ number of edge maps. This experiment uses two preprocessing algorithms, namely grayscale generation and Otsu thresholding, and six edge detectors, namely Sobel, Prewitt, Roberts, Canny, LoG and Zerocross obtained from MATLAB. Despite its trivial approach to generate a number of edge maps, this approach however is less effective to support the proposed performance evaluation due to the difficulties of any existing edge detector algorithm to generate optimal edges without any adjustment to its mechanism. The term 'adjustment' here refers to a set of preprocessing steps applied to input image which include the definition of threshold or other parameters required for the operation of edge detector, while the term 'optimal edge' refers to a complete closed-loop edge surrounding the object existed in digital image such as defined in the previous axioms. Employing Equation 14 to a set of USC standard test image would poorly produce optimal edges such as shown in Figure 6.

Therefore, other strategy for edge map generation is desired. Rather than obtaining edge maps directly from the combination of a set of preprocessing to a set of edge detectors, other approach is to generate a set of edge maps from the combination of other edge maps given by

$$\mathbf{EM}_r = \mathbf{EM}_s + \mathbf{EM}_t, \quad s \neq t \tag{15}$$

where $\mathbf{EM}_s$ and $\mathbf{EM}_t$ are generated by using Equation 14. Equation 15 produces more number of optimal edges such as shown in Figure 7. Although this approach would probably produce thick edges and violate the principle of non-maximal suppression, it is still considered as a better choice compared to obtaining edge maps with poor optimal edges. Moreover, any thick edges could easily be eliminated by using Axiom 2 as described above. By employing Equations 14 and 15, 66 different edge maps are obtained from each input image.

After generating a set of edge maps, the experiment is conducted by performing open-loop edge removal and edge thinning as defined in Equations 4–7. It is then continued with performance evaluation that generates sorted edge map from one with richest edges to the poorest by using both statistical-based and MCDM approach. The experiment produces 4 sorted edge maps from statistical-based approach based on edge length (EL), edge coverage (EC), object size (OA) and object coverage (OC), and 11 sorted edge maps generated by MCDM approach based on EL, EC, OA, OC, the combination of EL and EC (EL + EC), EL + OA, EL + OC, EC + OA, EC + OA, OA + OC, and EL + EC + OA + OC.

Validation to experimental results is held by comparing the result of sorted edge maps from different approaches against the ranking of edge maps selected by human observer. To simplify the comparison, only top 10 sorted edge maps from each approach are used in the validation stage, thus $N = 10$. In this experiment, a correlation test $C$ for purely indices data is developed to compare two sets of sorted edge maps as given by

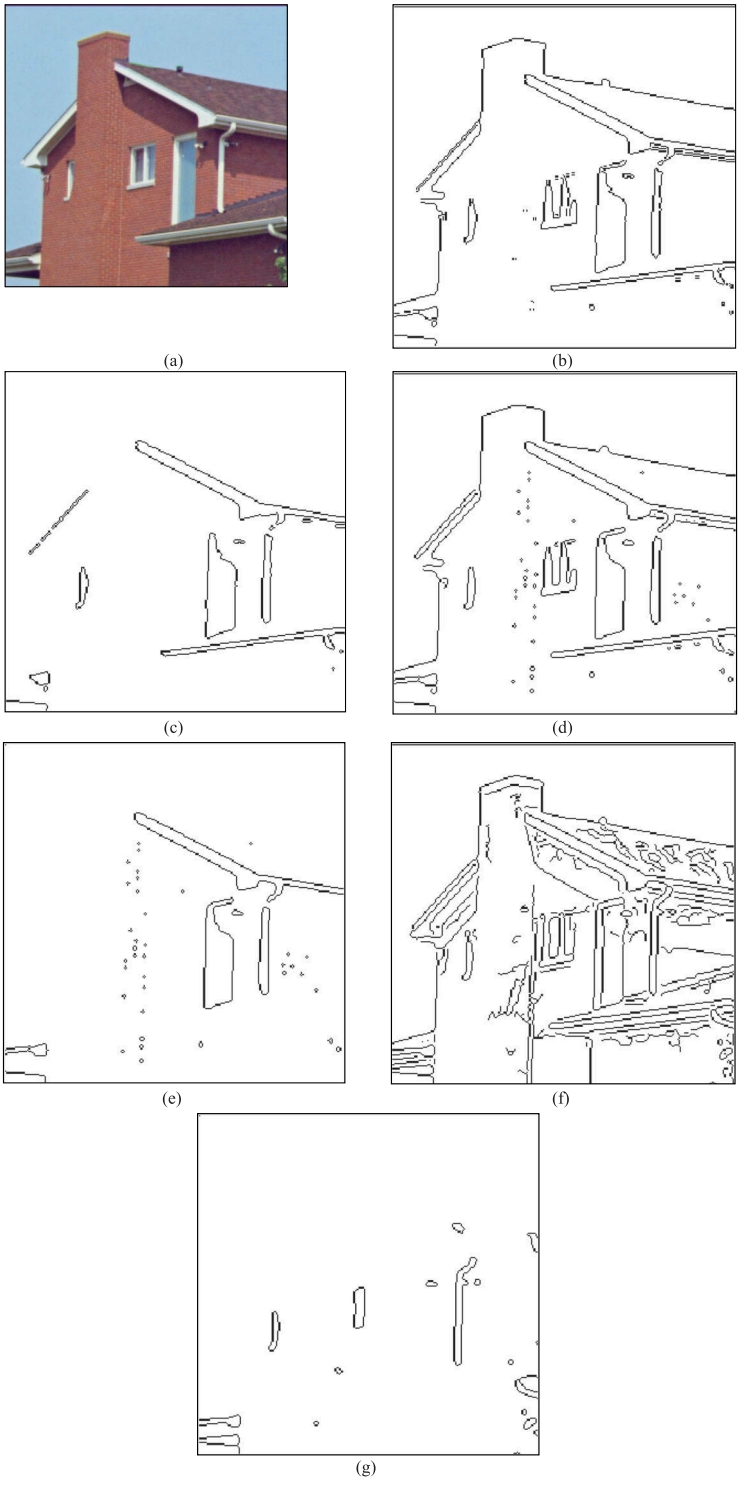


**Figure 6.** Result of Equation 11 to produce optimal edge. (a) Input, (b) edge detected by Equation 14 with Otsu threshold as preprocessing algorithm and Sobel edge detector, (c) closed-loop or optimal edge derived from (b), (d) similar to (b) with Otsu threshold and Canny edge detector, (e) optimal edge derived from (d), (f) similar to (b) with Grayscale and Canny and (g) optimal edge from (f).

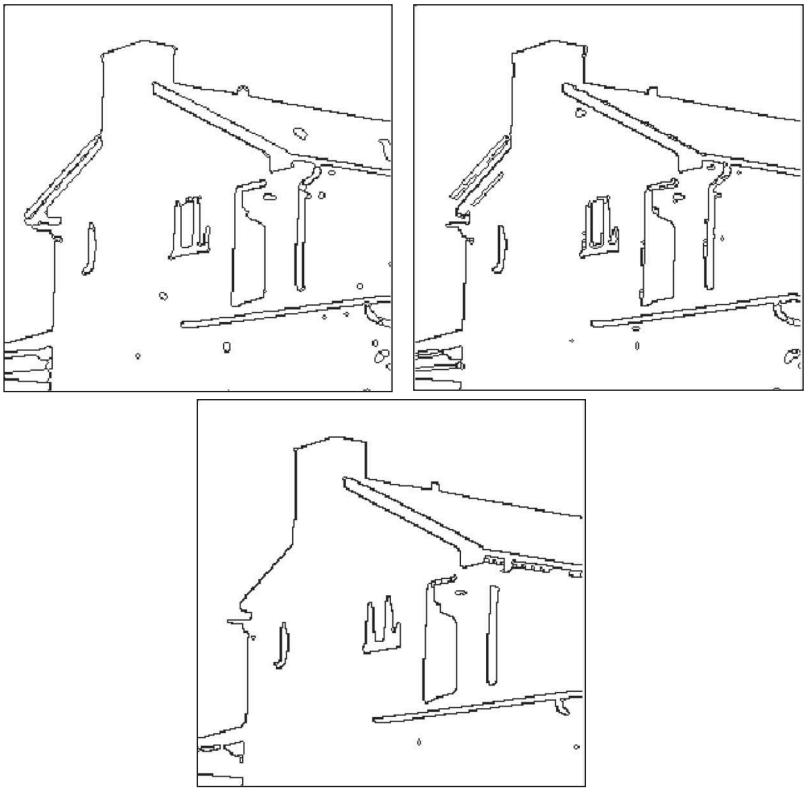

**Figure 7.** Various optimal edges obtained by using Equation 15 for the input as shown in Figure 6(a).

$$C = \sum_{i=1}^{N} \frac{x_i}{N} \tag{16}$$

where $x_i$ is generated by

$$x_i = \begin{cases} \frac{1}{|i-j|+1} & \text{for } d_i = r_j \\ 0 & \text{for } d_i \neq r_j \end{cases} \tag{17}$$

Here, $R = \{r_1, \ldots, r_N\}$ is the indices of sorted edge maps that become the reference for correlation test (in this case, it is the one selected by human observer) and $D = \{d_1, \ldots, d_N\}$ is the indices of sorted edge maps obtained from each approach. Equations 16 and 17 are required due to the fact that the data to be compared (i.e. $R$ and $D$) are purely indices that are originally generated by using Equations 14 and 15. These data could not be considered as categorical since the index is assigned iteratively in a looping process. In this case, each index is merely to label each edge map as the product of a unique process that does not represent any category or grouping of data. Moreover, negative correlation showing reversed connection between 2 datasets such as produced by many rank correlation coefficients is avoided in this experiment since the datasets are tested partially, i.e. involving only top 10 indices out of 66. Therefore, it is not possible to compute their correlation using

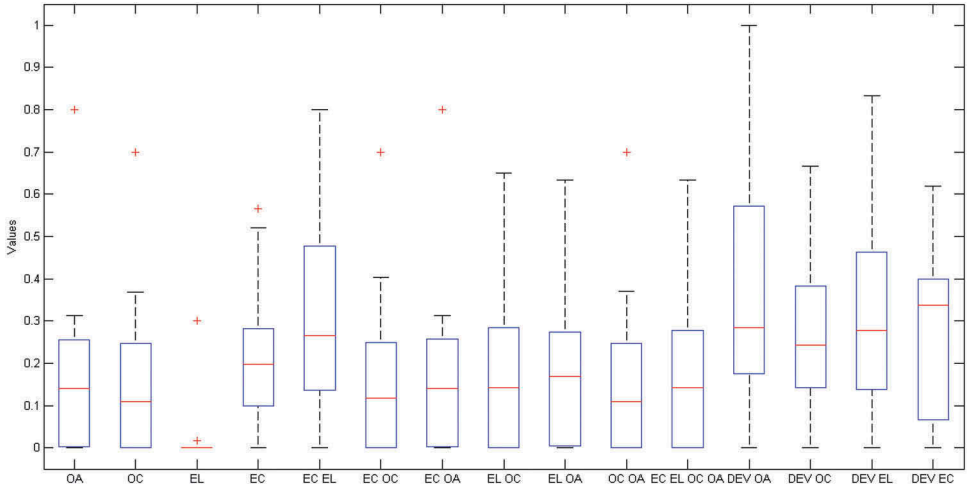


**Figure 8.** Result of correlation test from the presented approaches.

the existing rank correlation coefficients such as Pearson, Kendall or Spearman. Forcing to compute the correlation of experimental results using the existing methods would lead to misjudgement of index ranking since these methods treat each index as a numerical value. Detailed discussion of this issue however is beyond the scope of this paper and would be presented in a separate article.

Results of correlation test based on Equations 16 and 17 are presented in Figure 8, with its detail scores that are given in Table 1. This figure shows lower quartile, median, upper quartile and the outlier of correlation scores obtained by each approach. Based on Figure 8, five highest correlation scores with reference to human observer are obtained by four statistical approaches based on OA, EL, OC and EC, and an MCDM approach based on EL + EC.

At this point, however, it is still uncertain which approach among the top best five delivers the best performance since their presentation in Figure 8 is seemed indifferent in term of lower quartile, median and upper quartile. Therefore, it is necessary to conduct a statistical test on the mean average of correlation score. Hypothesis for statistical test is developed by drawing graphical presentation of sorted correlation score ($y$ axis) for all images ($x$ axis) used in the experiment from top best five approaches as depicted in Figure 9. This figure seems to show that statistical approach based on OA outperforms other approaches. Hence, a one-tail Student's $t$ distribution test with 95% confident level is then employed to validate this statement with the assumption that data in Table 1 are distributed normally. A set of hypothesis is then developed for this test as shown in the first and second column of Table 2 for $H_0$ and $H_1$, respectively. The result is shown in the third and forth column of Table 2.

Result of statistical test in Table 2 shows that correlation score of statistical approach based on OA is significantly higher than all other approaches. Meanwhile, correlation score of MCDM approach based on EL + EC is considered similar to statistical approach based on EL ($p$ value = 0.335741), and these two approaches are significantly higher

**Table 1.** Detailed result of correlation test from each approach.

| | MCDM approach | | | | | | | | | | | Statistical approach | | | |
|---|---|---|---|---|---|---|---|---|---|---|---|---|---|---|---|
| Data | $PI(\mathbf{OA})$ | $PI(\mathbf{OC})$ | $PI(\mathbf{EL})$ | $PI(\mathbf{EC})$ | $PI(\mathbf{EL},\mathbf{EC})$ | $PI(\mathbf{EC},\mathbf{OC})$ | $PI(\mathbf{EC},\mathbf{OA})$ | $PI(\mathbf{EL},\mathbf{OC})$ | $PI(\mathbf{EL},\mathbf{OA})$ | $PI(\mathbf{OC},\mathbf{OA})$ | $PI(\mathbf{EL},\mathbf{EC},\mathbf{OC},\mathbf{OA})$ | $\sigma(\mathbf{OA})$ | $\sigma(\mathbf{OC})$ | $\sigma(\mathbf{EL})$ | $\sigma(\mathbf{EC})$ |
| 1 | 0.18 | 0.18 | 0.30 | 0.25 | 0.58 | 0.18 | 0.28 | 0.28 | 0.28 | 0.18 | 0.28 | 0.57 | 0.35 | 0.57 | 0.35 |
| 2 | 0.10 | 0.10 | 0.00 | 0.24 | 0.25 | 0.10 | 0.10 | 0.10 | 0.10 | 0.10 | 0.10 | 0.32 | 0.15 | 0.32 | 0.23 |
| 3 | 0.26 | 0.25 | 0.00 | 0.13 | 0.19 | 0.25 | 0.26 | 0.25 | 0.25 | 0.25 | 0.25 | 0.34 | 0.32 | 0.19 | 0.34 |
| 4 | 0.28 | 0.22 | 0.00 | 0.52 | 0.63 | 0.22 | 0.28 | 0.33 | 0.43 | 0.23 | 0.28 | 0.21 | 0.44 | 0.63 | 0.44 |
| 5 | 0.26 | 0.37 | 0.00 | 0.24 | 0.23 | 0.37 | 0.26 | 0.37 | 0.26 | 0.36 | 0.36 | 0.45 | 0.26 | 0.23 | 0.39 |
| 6 | 0.00 | 0.00 | 0.00 | 0.07 | 0.48 | 0.00 | 0.00 | 0.00 | 0.00 | 0.00 | 0.00 | 0.68 | 0.47 | 0.48 | 0.04 |
| 7 | 0.00 | 0.00 | 0.00 | 0.14 | 0.80 | 0.00 | 0.00 | 0.00 | 0.00 | 0.00 | 0.00 | 1.00 | 0.24 | 0.53 | 0.36 |
| 8 | 0.00 | 0.00 | 0.00 | 0.18 | 0.13 | 0.00 | 0.00 | 0.00 | 0.00 | 0.00 | 0.00 | 0.26 | 0.23 | 0.13 | 0.43 |
| 9 | 0.02 | 0.02 | 0.00 | 0.31 | 0.45 | 0.02 | 0.02 | 0.02 | 0.02 | 0.02 | 0.02 | 0.47 | 0.35 | 0.45 | 0.62 |
| 10 | 0.15 | 0.07 | 0.00 | 0.03 | 0.00 | 0.07 | 0.15 | 0.04 | 0.11 | 0.07 | 0.06 | 0.07 | 0.07 | 0.07 | 0.07 |
| 11 | 0.00 | 0.00 | 0.00 | 0.08 | 0.57 | 0.00 | 0.00 | 0.00 | 0.00 | 0.00 | 0.00 | 1.00 | 0.64 | 0.57 | 0.14 |
| 12 | 0.18 | 0.18 | 0.00 | 0.24 | 0.37 | 0.18 | 0.18 | 0.18 | 0.19 | 0.18 | 0.18 | 1.00 | 0.44 | 0.28 | 0.56 |
| 13 | 0.13 | 0.11 | 0.00 | 0.17 | 0.24 | 0.13 | 0.13 | 0.13 | 0.24 | 0.11 | 0.14 | 0.29 | 0.39 | 0.18 | 0.34 |
| 14 | 0.30 | 0.30 | 0.00 | 0.43 | 0.27 | 0.30 | 0.30 | 0.30 | 0.30 | 0.30 | 0.30 | 0.26 | 0.14 | 0.09 | 0.43 |
| 15 | 0.17 | 0.17 | 0.00 | 0.36 | 0.35 | 0.17 | 0.17 | 0.17 | 0.17 | 0.17 | 0.17 | 0.78 | 0.54 | 0.35 | 0.40 |
| 16 | 0.24 | 0.24 | 0.00 | 0.20 | 0.33 | 0.25 | 0.25 | 0.26 | 0.26 | 0.24 | 0.24 | 0.27 | 0.27 | 0.33 | 0.23 |
| 17 | 0.09 | 0.09 | 0.00 | 0.00 | 0.68 | 0.09 | 0.09 | 0.14 | 0.14 | 0.09 | 0.09 | 0.20 | 0.20 | 0.42 | 0.17 |
| 18 | 0.27 | 0.27 | 0.00 | 0.35 | 0.70 | 0.27 | 0.27 | 0.29 | 0.32 | 0.37 | 0.27 | 0.67 | 0.67 | 0.70 | 0.35 |
| 19 | 0.80 | 0.70 | 0.00 | 0.57 | 0.47 | 0.70 | 0.80 | 0.65 | 0.63 | 0.70 | 0.63 | 0.57 | 0.53 | 0.47 | 0.57 |
| 20 | 0.05 | 0.04 | 0.00 | 0.05 | 0.08 | 0.07 | 0.05 | 0.20 | 0.20 | 0.05 | 0.20 | 0.05 | 0.17 | 0.08 | 0.05 |
| 21 | 0.25 | 0.30 | 0.00 | 0.48 | 0.67 | 0.40 | 0.25 | 0.40 | 0.40 | 0.25 | 0.40 | 0.67 | 0.33 | 0.83 | 0.48 |
| 22 | 0.07 | 0.07 | 0.00 | 0.10 | 0.08 | 0.07 | 0.07 | 0.07 | 0.07 | 0.07 | 0.07 | 0.17 | 0.23 | 0.07 | 0.12 |
| 23 | 0.24 | 0.22 | 0.00 | 0.25 | 0.16 | 0.21 | 0.20 | 0.28 | 0.24 | 0.22 | 0.24 | 0.25 | 0.22 | 0.17 | 0.25 |
| 24 | 0.26 | 0.26 | 0.00 | 0.29 | 0.32 | 0.26 | 0.26 | 0.29 | 0.29 | 0.26 | 0.29 | 0.30 | 0.32 | 0.32 | 0.40 |
| 25 | 0.14 | 0.12 | 0.00 | 0.04 | 0.00 | 0.12 | 0.14 | 0.12 | 0.15 | 0.12 | 0.12 | 0.00 | 0.00 | 0.20 | 0.07 |
| 26 | 0.31 | 0.31 | 0.00 | 0.13 | 0.00 | 0.31 | 0.31 | 0.31 | 0.31 | 0.31 | 0.31 | 0.31 | 0.04 | 0.00 | 0.02 |
| 27 | 0.01 | 0.00 | 0.02 | 0.10 | 0.00 | 0.00 | 0.01 | 0.00 | 0.00 | 0.00 | 0.00 | 0.00 | 0.00 | 0.00 | 0.00 |
| 28 | 0.00 | 0.00 | 0.00 | 0.18 | 0.18 | 0.00 | 0.00 | 0.00 | 0.00 | 0.00 | 0.00 | 0.10 | 0.24 | 0.37 | 0.38 |
| 29 | 0.00 | 0.00 | 0.00 | 0.21 | 0.17 | 0.00 | 0.00 | 0.00 | 0.00 | 0.00 | 0.00 | 0.07 | 0.02 | 0.27 | 0.01 |
| 30 | 0.00 | 0.00 | 0.00 | 0.20 | 0.27 | 0.00 | 0.00 | 0.00 | 0.02 | 0.00 | 0.00 | 0.20 | 0.03 | 0.25 | 0.00 |
| $\mu(C)$ | **0.16** | **0.15** | **0.01** | **0.22** | **0.32** | **0.16** | **0.16** | **0.17** | **0.18** | **0.16** | **0.17** | **0.38** | **0.28** | **0.32** | **0.27** |

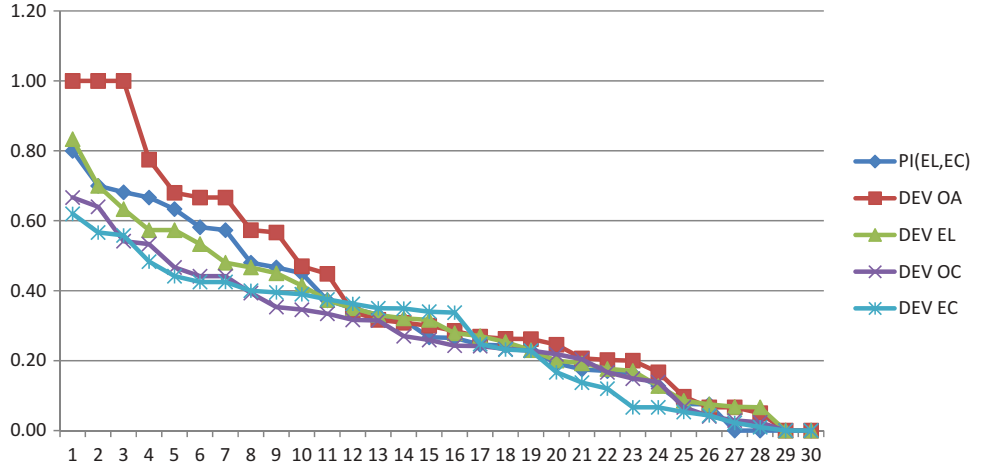


**Figure 9.** Sorted correlation score of five top best approaches.

**Table 2.** Hypothesis and result of Student's *t* distribution test on correlation score.

| $H_0$ | $H_1$ | *p* Value | Result |
|---|---|---|---|
| $\mu(C_{\sigma(OA)}) \leq \mu(C_{PI(EL,EC)})$ | $\mu(C_{\sigma(OA)}) > \mu(C_{PI(EL,EC)})$ | 0.000118 | 1 |
| $\mu(C_{\sigma(OA)}) \leq \mu(C_{\sigma(EL)})$ | $\mu(C_{\sigma(OA)}) > \mu(C_{\sigma(EL)})$ | 0.000482 | 1 |
| $\mu(C_{\sigma(OA)}) \leq \mu(C_{\sigma(OC)})$ | $\mu(C_{\sigma(OA)}) > \mu(C_{\sigma(OC)})$ | 0.000027 | 1 |
| $\mu(C_{\sigma(OA)}) \leq \mu(C_{\sigma(EC)})$ | $\mu(C_{\sigma(OA)}) > \mu(C_{\sigma(EC)})$ | 0.000087 | 1 |
| $\mu(C_{PI(EL,EC)}) \leq \mu(C_{\sigma(EL)})$ | $\mu(C_{PI(EL,EC)}) > \mu(C_{\sigma(EL)})$ | 0.335741 | 0 |
| $\mu(C_{PI(EL,EC)}) \leq \mu(C_{\sigma(OC)})$ | $\mu(C_{PI(EL,EC)}) > \mu(C_{\sigma(OC)})$ | 0.000191 | 1 |
| $\mu(C_{PI(EL,EC)}) \leq \mu(C_{\sigma(EC)})$ | $\mu(C_{PI(EL,EC)}) > \mu(C_{s(EC)})$ | 0.000837 | 1 |
| $\mu(C_{\sigma(EL)}) \leq \mu(C_{\sigma(OC)})$ | $\mu(C_{\sigma(EL)}) > \mu(C_{\sigma(OC)})$ | 0.000003 | 1 |
| $\mu(C_{\sigma(EL)}) \leq \mu(C_{\sigma(EC)})$ | $\mu(C_{\sigma(EL)}) > \mu(C_{\sigma(EC)})$ | 0.000095 | 1 |
| $\mu(C_{\sigma(OC)}) \leq \mu(C_{\sigma(EC)})$ | $\mu(C_{\sigma(OC)}) > \mu(C_{\sigma(EC)})$ | 0.364214 | 0 |

than statistical approach based on both OC and EC. Finally statistical approach based on OC is considered indifferent to statistical approach based on EC (*p* value = 0.364214).

Correlation and statistical test above prove that statistical approach based on OA delivers higher performance among other methods. The correlation score depicted in Figure 8 shows that in the average, the presented approaches achieve low correlation to human observer as shown by low median value ($C<0.4$) from 0 to 1 range of correlation score. Localising low correlation score ($C<0.4$) obtained by statistical approach based on OA as previously presented in Table 1 from high correlation score ($C \geq 0.4$), such as shown in Table 3, reveals the following phenomenon. There is significant number of images suffering from fail detection of main objects in both categories, i.e. 15.79% (3/19) and 18.18% (2/11) from low and high correlation, respectively.

However, focus of the analysis here is on large number of images in low correlation category which suffer from disagreement between human observers against the presented algorithm to perceive the structure of edge, i.e. as much as 78.95% (15/19). It is caused by high complexity of image scenes that contain multiple objects or an object with multiple components in similar sizes such as shown in Figure 10.

**Table 3.** Classifying correlation score.

| | | Retrieval success[a] | |
|---|---|---|---|
| Correlation score | Fail to retrieve main object | Disagree | Agree |
| $C < 0.4$ | 3 | 15 | 1 |
| $C \geq 0.4$ | 2 | 1 | 8 |

[a]Disagree and agree is measured by the agreement between human observer and the presented algorithms to select best edge map.

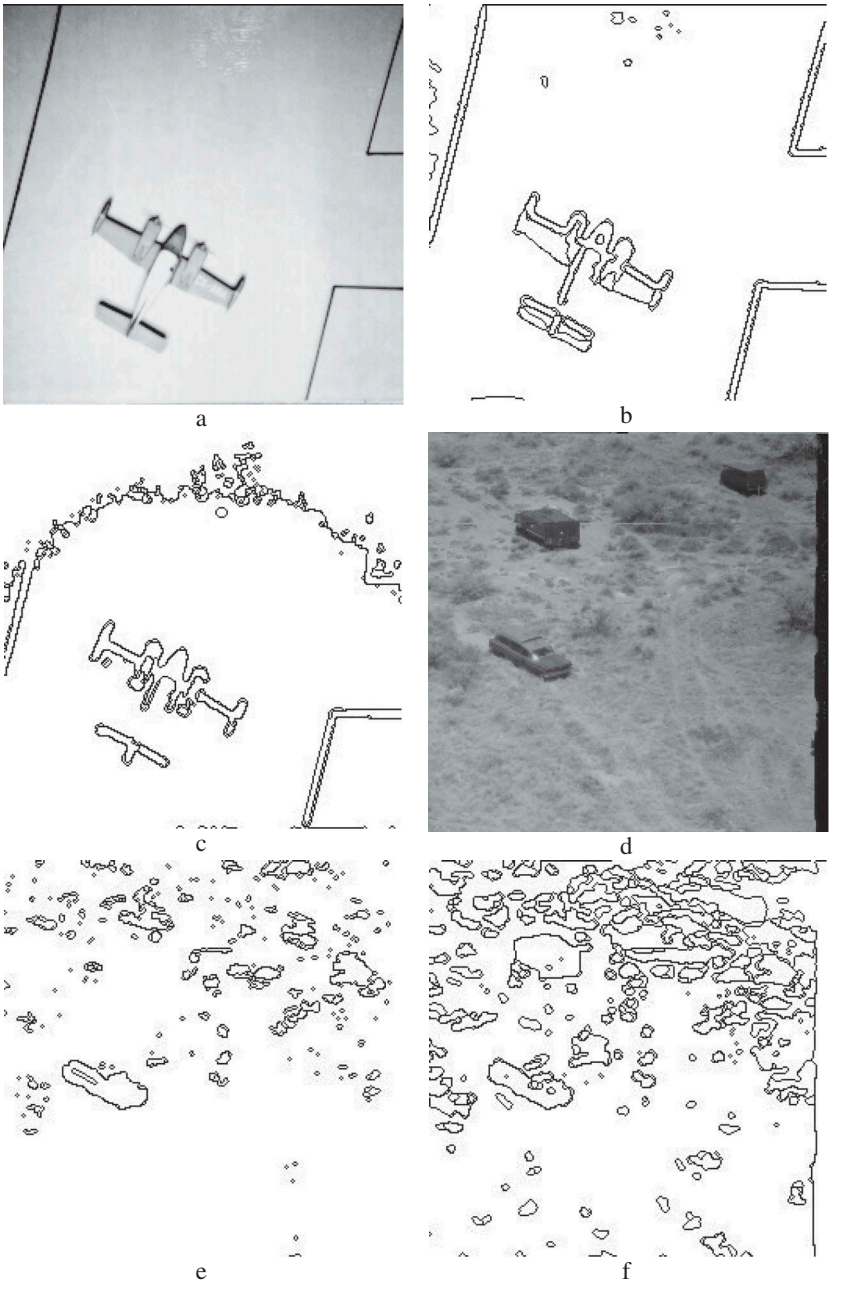


**Figure 10.** Difference results of first-rank edge map selected by human versus machine. Figure parts (a,d,g,j,m) are input images, (b,e,h,k,n) are edge map selected by human observer and (c,f,i,l,o) are selected by OA-based statistical approach.

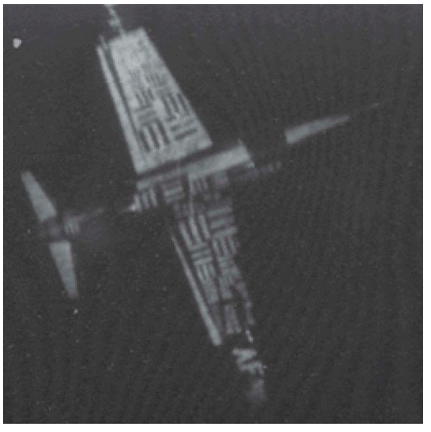

g

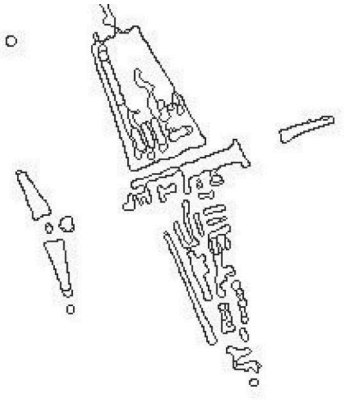

h

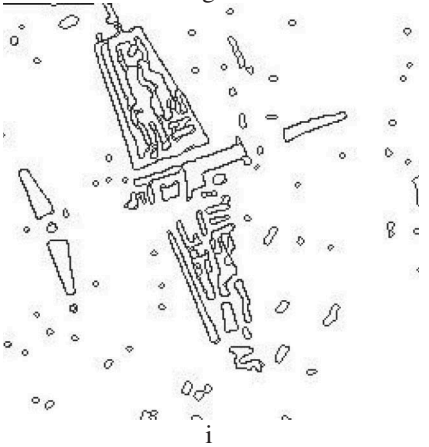

i

j

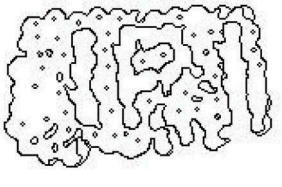

k

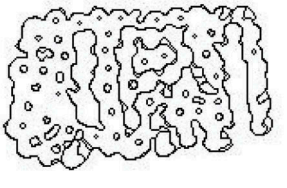

l

**Figure 10.** Continued.

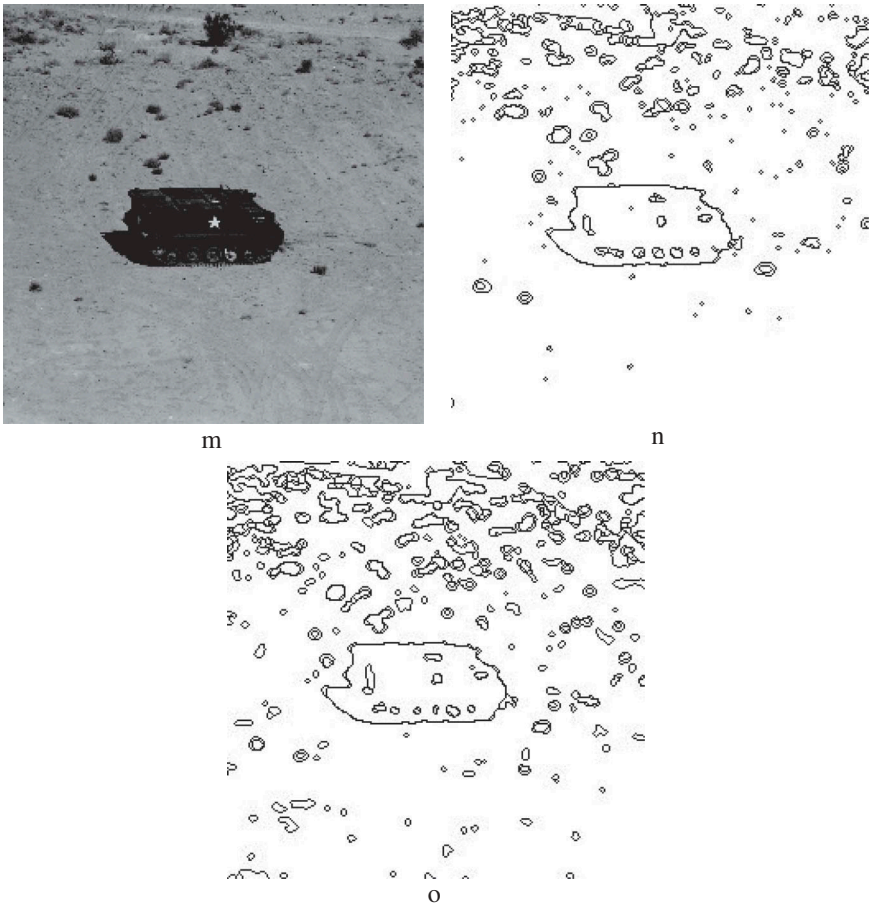


**Figure 10.** Continued.

Varied edge structures are produced by different combination of edge detectors from this type of images. Moreover, the images as shown in Figure 10 contain objects that do not dominate the scene due to small object size relative to the size of other objects and its background. Hence, the evaluations of edge map by human and machine are conducted differently based on their nature of data processing. In this case, the machine computes every detail numerical values from all edges in order to measure their performance, while in reality, human visual system is capable of focusing on only an object for every single sight. Therefore, human tends to simplify edges and focuses on the main objects.

Different condition is found when image complexity is lower, i.e. edge detectors successfully deliver complete closed-loop edge from the main object that hold dominant size compared to other object such as shown in Figure 11. In this case, both human and machine agree to select the same edge map at the top. Thus, it is important to reduce scene complexity by defining region of interest (ROI) in order to imitate human vision. Manual assignment of ROI to some image data with high scene

complexity such as shown in Figure 12 greatly improves the correlation value as shown in Figure 13. In this measurement from 14 image data with high complexity, ROI is capable of improving both mean and median of correlation value from 0.1633 and 0.1833, respectively, to become 0.5578 and 0.61, respectively.

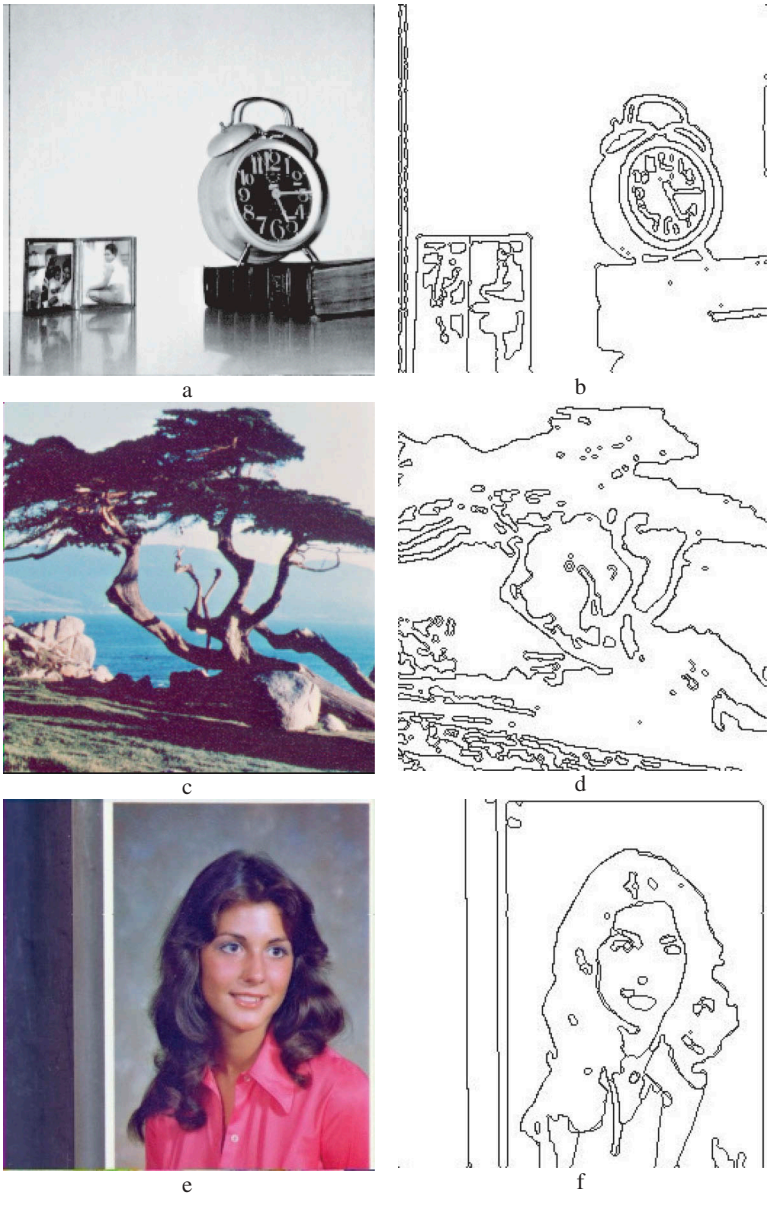


**Figure 11.** The same result of best edge map selection by human and machine for image with lower scene complexity. Figure parts (a,c,e,g,i) are input images and (b,d,f,h,j,) are best edge map selected by both human observer and OA-based statistical approach.

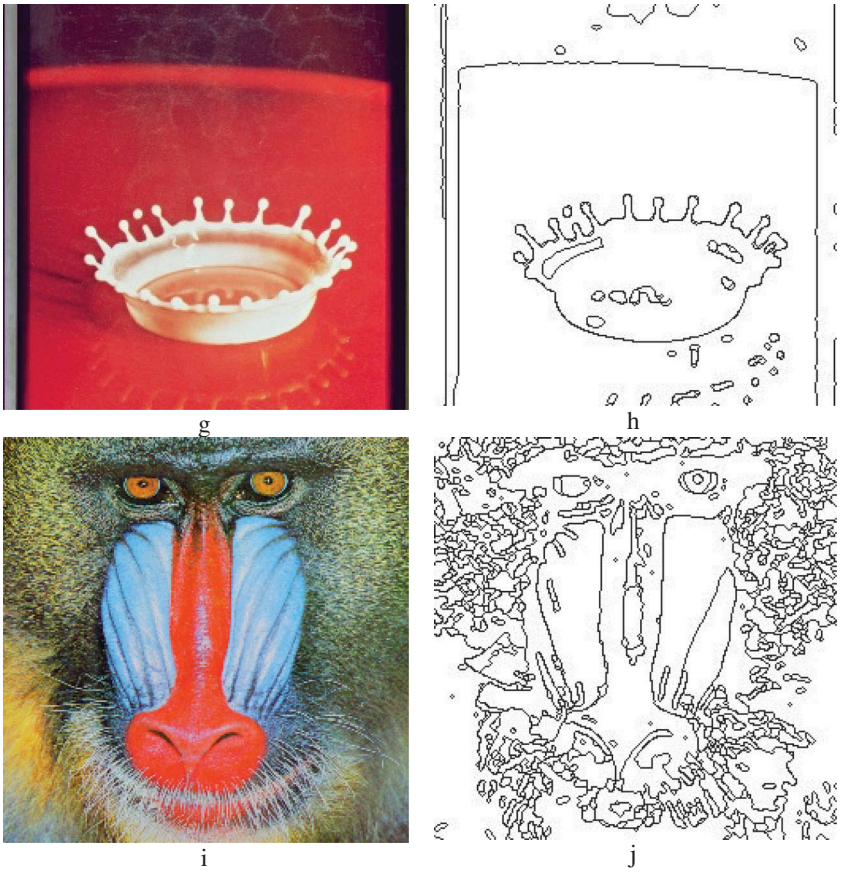


**Figure 11.** Continued.

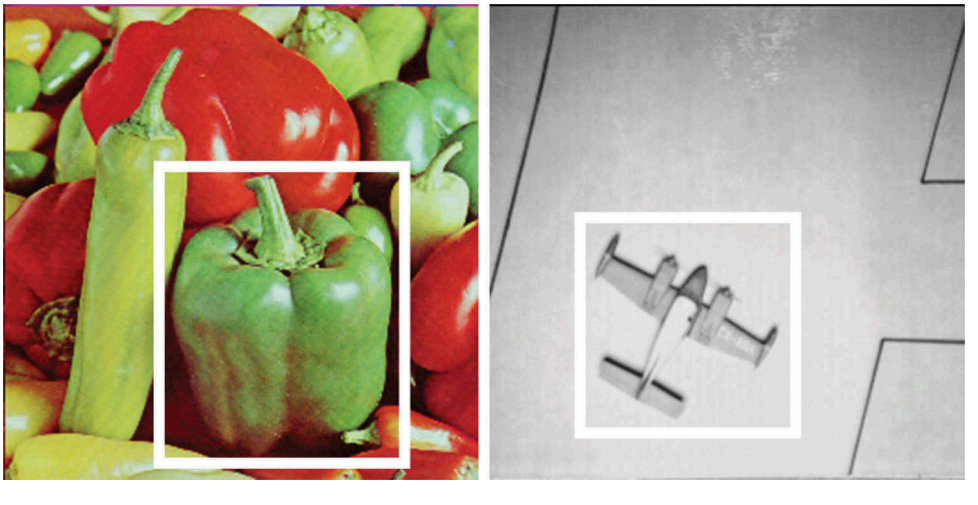

**Figure 12.** ROI assignment (in white box).

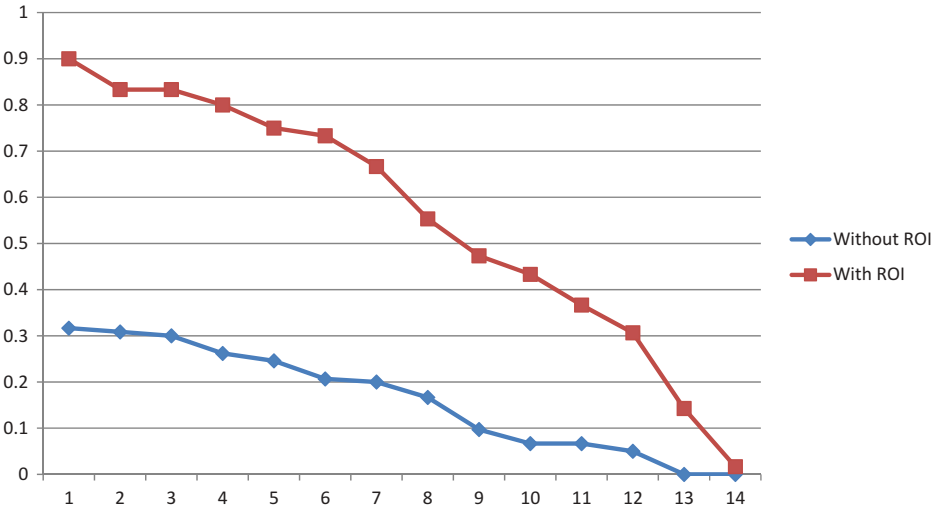


**Figure 13.** Sorted correlation value without and with ROI assignment to some image data.

## 6. Conclusion

The existing algorithms of edge detector still suffer from incomplete edge detection from varied objects contained in natural image scenes. It is different to human vision that is capable of always recognising closed-loop edges from even complicated and noisy scenes. Although human and machine employs similar approach to measure the changes of intensity, colour or other local parameters as the indication of edge, human develops more sophisticated intelligence to build complete closed-loop edges from the perception of object in a scene. In this case, lack of intelligence in machine often violates the presence of edge. For instance, the exaggeration of inner attributes of an object such as its texture or ridges by lighting would most probably create stronger changes of intensity than the boundary of object. Due to this condition, the research employs a removal approach to eliminate open-loop edges in order to obtain the best edge detector. The approach forces edge detector that is incapable of delivering closed-loop edges to loss the presence of object. It is similar to human vision suffering from short sighted but is forced to view distance object. Hence, the performance is measured based on the knowledge of edge detector to retrieve the presence of object. Experimental result shows that statistical approach based on the size of object becomes the best approach compared to other presented algorithms. The experiment also proves useful application of ROI to simplify the complexity of image scene in order to optimise performance measurement.

## ORCID

Cahyo Crysdian http://orcid.org/0000-0002-7488-6217

## References

Abdou, K.E. and Pratt, W.K., 1979. Quantitative design and evaluation of enhancement/thresholding edge detectors. *Proceedings of IEEE*, 67 (5), 753–763. doi:10.1109/PROC.1979.11325

Baddeley, A.J., 1992. An error metric for binary images. Proc. of the Int. Workshop on Robust Computer Vision, Bonn, 1992, 59-78.

Besuijen, J. and Heyden, F., 1989. An edge detection performance measure incorporating structural errors. *Douzieme Colloque Gretsi - Juan-Les-Pins 12 AU*, 16 (June), 1989.

Desolneux, A., Moisan, L., and Morel, J.M. 2008. From gestalt theory to image analysis: a probabilistic approach. In: *Springer-verlag collection, interdisciplinary applied mathematics*, Vol. 34. New York: Springer-Verlag. ISBN: 978-0-387-72635-9.

Gimenez, J., Martinez, J., and Flesia, A.G., 2014. Unsupervised edge map scoring: a statistical complexity approach. *Computer Vision and Image Understanding (Elsevier)*, 122, 131–142. doi:10.1016/j.cviu.2014.02.005

Hidalgo, M.G. and Massanet, S., 2011. Towards an objective edge detection algorithm based on discrete t-norms. *In:* Galichet S, Montero J, Mauris G, eds. *Proceedings of the 7th conference of the european society for fuzzy logic and technology (EUSFLAT-2011) and LFA-2011, Advances in Intelligent Systems Research*, 319–326.

Ji, Q. and Haralick, R.M., 1999. Quantitative evaluation of edge detectors using the minimum kernel variance criterion. IEEE International Conference on Image Processing, Volume 2, 1999, 705-709.

Koren, R. and Yitzhaky, Y., 2006. Automatic selection of edge detector parameters based on spatial and statistical measures. *Computer Vision and Image Understanding (Elsevier)*, 102, 204–213. doi:10.1016/j.cviu.2006.01.005

Oliva, A. and Torralba, A., 2006. Building the gist of a scene: the role of global image features in recognition. *Progress in Brain Research (Elsevier)*, 155, 23–36.

Ornelas, F.P., *et al*., 2015. Fuzzy index to evaluate edge detection in digital images. *PLoS ONE*, 10 (6), e0131161. doi:10.1371/journal.pone.0131161

Oskoei, M.A. and Hu, H., 2010. A survey on edge detection methods. *Technical Report: CES-506, ISSN 1744 – 8050*. Colchester: School of Computer Science & Electronic Engineering, University of Essex.

Papari, G. and Petkov, N., 2011. Edge and line oriented contour detection: state of the art. *Image and Vision Computing (Elsevier)*, 29 (2–3), 79–103. doi:10.1016/j.imavis.2010.08.009

Verma, O.P., *et al*., 2011. A novel bacterial foraging technique for edge detection. *Pattern Recognition Letters (Elsevier)*, 32 (8), 1187–1196. doi:10.1016/j.patrec.2011.03.008

Yitzhaky, Y. and Peli, E., 2003. A method for objective edge detection evaluation and detector parameter selection. *IEEE Transactions on Pattern Analysis and Machine Intelligence*, 25 (8), 1027–1033. August. doi:10.1109/TPAMI.2003.1217608

Zhang, T.Y. and Suen, C.Y., 1984. A fast parallel algorithm for thinning digital patterns. *Image Processing and Computer Vision, Communications of the ACM*, 27 (8), 236–239. March.